Chirality-Induced Spin Currents in a Fermi Gas

Camen A. Royse and J. E. Thomas
Department of Physics, North Carolina State University, Raleigh, North Carolina 27695, USA

(Received 29 October 2025; revised 20 January 2026; accepted 26 February 2026; published 23 March 2026)

We observe and model spin currents arising from chirality and effective spin-exchange interactions in a weakly interacting ^{6}Li Fermi gas. Chirality is introduced by a static displacement between the center of the trapped atoms and the center of an applied magnetic bowl, which produces left- or right-handed spatially varying spin rotation. Spin current is directly observed via oscillations in the centers of mass of the spin-up and spin-down components, which appear to bounce off of or pass through one another, depending on the degree of handedness and s-wave scattering length. We show that this behavior obeys a driven oscillator equation with an effective spin-dependent driving force. Our measurements demonstrate chirality-induced spin selectivity via the direction of the current flow, extending CISS phenomena to Fermi gases.

DOI: 10.1103/73th-7hwt

Chiral (twisted) materials are of great interest for generating and controlling spin-polarized electron currents [1] to enable "spintronics" technologies. In such technologies, information is transmitted via spin currents instead of electron currents, greatly reducing Joule heating, which limits the scalability of computers. Chiral molecules [2] can act as passive spin filters, efficiently transporting electrons for one polarization while impeding the transmission of the other. Large chiral-induced spin selectivity (CISS) has been observed in the asymmetric transmission of polarized electrons through thin films of chiral molecules, including DNA [3,4]. While spin-orbit coupling is known to play a role in this effect, no unifying theory of the role of chirality has been able to quantitatively reproduce measurements. Spin transport in chiral materials is now widely studied [5–8] for manipulating spin-selective currents. Ultracold Fermi gases provide experimental simulators for spintronics concepts [9], which may offer new insights into chiral control methods.

We directly observe chirality-induced spin currents in a trapped, weakly interacting Fermi gas of ^{6}Li atoms confined in the combined potential of a cigar-shaped CO_2 laser trap and a magnetic bowl (Fig. 1). In contrast to chiral materials, where twist is structural, a chiral spin texture (i.e., a spin spiral or twist) is created in the cloud by simply displacing the center of the laser trap from the center of the magnetic bowl, which causes the coherently prepared spin medium to evolve into a twisted state. We show that the spin centers of mass obey a 1D driven oscillator equation, where an effective spin-dependent driving force arises from s-wave scattering in the twisted medium and is tunable from aperiodic to impulsive.

The ^{6}Li atoms are initially prepared in a z-polarized spin state $|\uparrow\rangle$. A 0.5 ms $\pi/2$ rf pulse then creates a pseudospin state [10], which we define to be x-polarized, $(|\uparrow\rangle + |\downarrow\rangle)/\sqrt{2}$, where $|\uparrow\rangle, |\downarrow\rangle$ denote the two lowest hyperfine states, in order of increasing energy. A bias magnetic field B_z (orthogonal to the trap axis x) both defines the quantization axis and controls spin-spin interactions by tuning the $|\uparrow\rangle - |\downarrow\rangle$ s-wave scattering length a_s. Key to the experiments is the curvature of $B_z(x)$, which creates a spin-dependent harmonic potential (i.e., a magnetic bowl) that confines the cloud along the x-axis, with negligible effect in the narrow transverse directions y, z. The CO_2 laser potential provides radial confinement and has a relatively short Rayleigh length, $\simeq$0.75 mm, producing a spin-independent axial force that is comparable to that of the magnetic bowl. The center of the magnetic bowl is determined by fixed electromagnets, while the CO_2 laser focal point is easily translated to shift the center of the trapped atoms relative to that of the magnetic bowl.

The net optical and magnetic axial potential is

$$V_{\uparrow,\downarrow}(x) = \frac{m\omega_0^2}{2}x^2 \pm \frac{m\omega_0\delta\omega_{\uparrow\downarrow}}{2}(x - x_{os})^2, \qquad (1)$$

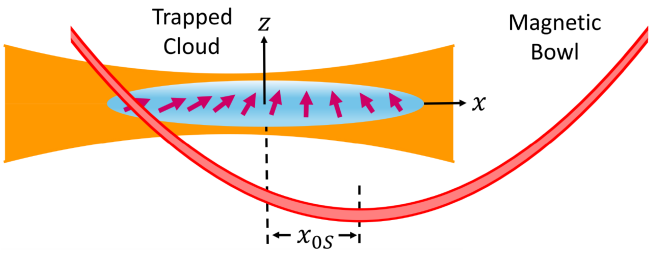

FIG. 1. Controlling spin twist in an atomic Fermi gas. A cigar-shaped cloud of ^{6}Li (light blue), prepared in a superposition of spin-up and spin-down states, is confined by a focused CO_2 laser beam (orange) and a magnetic bowl (red). The x-dependent spin twist about the chiral z-axis is controlled by the offset x_{os} between the centers of the spin-dependent magnetic bowl potential and the trapped cloud (blue) at $x \equiv 0$.

where $\omega_0 \equiv 2\pi\nu_x \simeq 2\pi \times 25$ Hz is the average harmonic oscillation frequency, and $\delta\omega_{\uparrow\downarrow} \simeq 2\pi \times 14$ mHz is the difference in the harmonic oscillation frequencies for the two states [11]. Note that the small value of $\delta\omega_{\uparrow\downarrow}/\omega_0$ is due to the fact that the two states differ only in nuclear spin projection. The average potential is spin independent and centered at $x \equiv 0$. Chirality is controlled by x_{os}, the offset between the measured centers of the magnetic bowl and the trapped cloud.

In equilibrium, $F_{\uparrow,\downarrow} = -\partial_x V_{\uparrow,\downarrow}(x) = 0$, the displacement between the centers of the density profiles $n_\uparrow$ and $n_\downarrow$, to first order in $\delta\omega_{\uparrow\downarrow}/\omega_0$, is

$$x_\uparrow - x_\downarrow = \frac{2\delta\omega_{\uparrow\downarrow}}{\omega_0} x_{os}. \tag{2}$$

For our experiments, where $x_{os} \simeq \sigma_x \simeq 200$ μm, we find $x_\uparrow - x_\downarrow \simeq 0.2$ μm, which is negligible compared to the cloud widths. We observe no difference in the positions of pure $|\uparrow\rangle$ or $|\downarrow\rangle$ states in the trap. Hence, the difference between the mechanical forces does not play a role in the evolution of the system. However, the spatially varying frequency shift $(V_\uparrow - V_\downarrow)/\hbar$ produces a spatially varying rotation rate of the pseudospins about the chiral z-axis

$$\mathbf{\Omega} = \hat{\mathbf{z}}\,\Omega_0 \frac{(x - x_{os})^2}{\sigma_x^2}, \tag{3}$$

in a frame rotating at the hyperfine resonance frequency, creating a twisted spin state as the system evolves [13]. Here, $\Omega_0 \equiv m\omega_0\delta\omega_{\uparrow\downarrow}\sigma_x^2/\hbar = 52.6\ s^{-1}$ at 511 G for $\sigma_x = 198$ μm [14]. Ω_0 is determined by the known magnetic field tuning rate for each state and the measured oscillation frequency of atoms in the magnetic bowl $\omega_{\rm mag}$ [11].

Just after the $\pi/2$ pulse, all of the spins are parallel [10], and hence, noninteracting in a Fermi gas restricted to s-wave scattering. The initial evolution of the pseudospins is then governed by the x-dependent rotation rate $\mathbf{\Omega}$, causing the spin vectors to point in different directions at a later time, enabling scattering interactions between the atoms. In the weakly interacting regime, the atoms remain in simple harmonic motion. However, forward s-wave scattering between atoms with nonparallel spins causes each spin vector to rotate about the total spin vector [19–22], analogous to a spin-exchange interaction, which produces a measurable spin z component.

We investigate the interplay between the interaction strength, controlled by the s-wave scattering length a_s, and the chirality, controlled by the offset x_{os}. Asymmetric spatial profiles are observed for nonzero static displacements x_{os}, as shown in Fig. 2. The experiments are performed in the nondegenerate regime, where the reduced temperature $0.5 < T/T_F < 0.7$. The profiles of both spin states are identical immediately after the rf pulse and nominally Gaussian, centered at $x = 0$ with a $1/e$ width $\sigma_x \simeq 200$ μm [14].

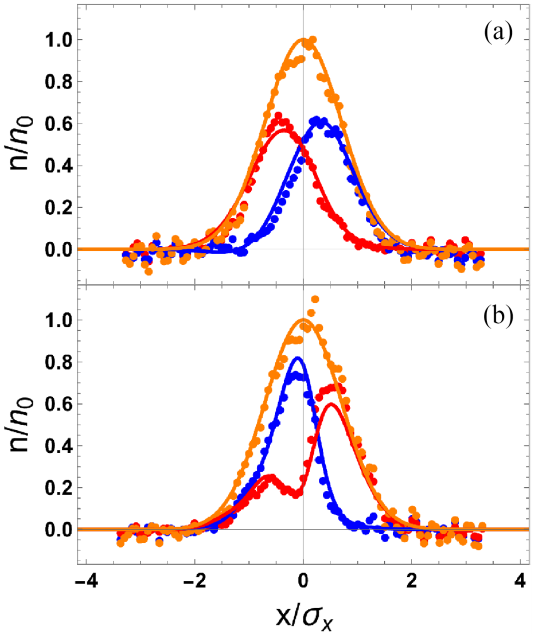

FIG. 2. Spatial profiles for spin-up and spin-down states. Spin-up (blue), spin-down (red). The total density $n_\uparrow + n_\downarrow$ (orange) is conserved. Chirality is controlled by the offset parameter x_{os}; see Fig. 1. (a) $x_{os} = 1.0\sigma_x$ at $t = 21$ ms with an s-wave scattering length $a_s = -53.1a_0$ G; (b) $x_{os} = -0.9\sigma_x$ at $t = 37$ ms for $a_s = -213.1a_0$. Predictions (solid curves).

Figure 2(a) shows density profiles for $x_{os} = 1.0\sigma_x$ at $B = 511$ G, where the s-wave scattering length $a_s = -53.1a_0$, the peak total density $\bar{n}_0 = 0.90/\mu\text{m}^3$ (see below), and the trap frequency $\nu_x = 25.9$ Hz. At $t = 21$ ms after the $\pi/2$ rf pulse (about half of the trap period), the spin-up profile (blue) is shifted to the right, while the spin-down profile (red) is shifted left [23]. Figure 2(b) shows the results obtained for negative $x_{os} = -0.9\sigma_x$ with at $B = 437$ G, where $a_s = -213.1a_0$, $\bar{n}_0 = 0.52/\mu\text{m}^3$, and $\nu_x = 24.3$ Hz. At $t = 37$ ms, the profile of the spin-up (blue) is shifted to the left, while that of the spin-down component (red) is distorted on the left and shifted right. In both cases, the total spin density $n(x) = n_\uparrow(x,t) + n_\downarrow(x,t)$ is time independent and remains a Gaussian centered at $x = 0$ (orange), demonstrating spin current without total density (charge) current. Solid curves show the predictions of the model, discussed below.

We quantify the effect of chirality on the motion by plotting the center of mass $\langle x\rangle_{\uparrow,\downarrow} = \int dx x n_{\uparrow,\downarrow}(x,t)/N_{\uparrow,\downarrow}$ for each state versus time for different offsets x_{os}. Figure 3 shows data for x_{os} of $0.8\sigma_x, 0, -0.8\sigma_x$, and $-3\sigma_x$ at 511 G, where $a_s = -53.1a_0$. Figure 3(b) locates the center of the magnetic bowl, $x_{os} = 0$, where there is no separation in the centers of mass. For $x_{os} \neq 0$, the centers of mass exhibit 180° out-of-phase spin-dipole modes. The directions of

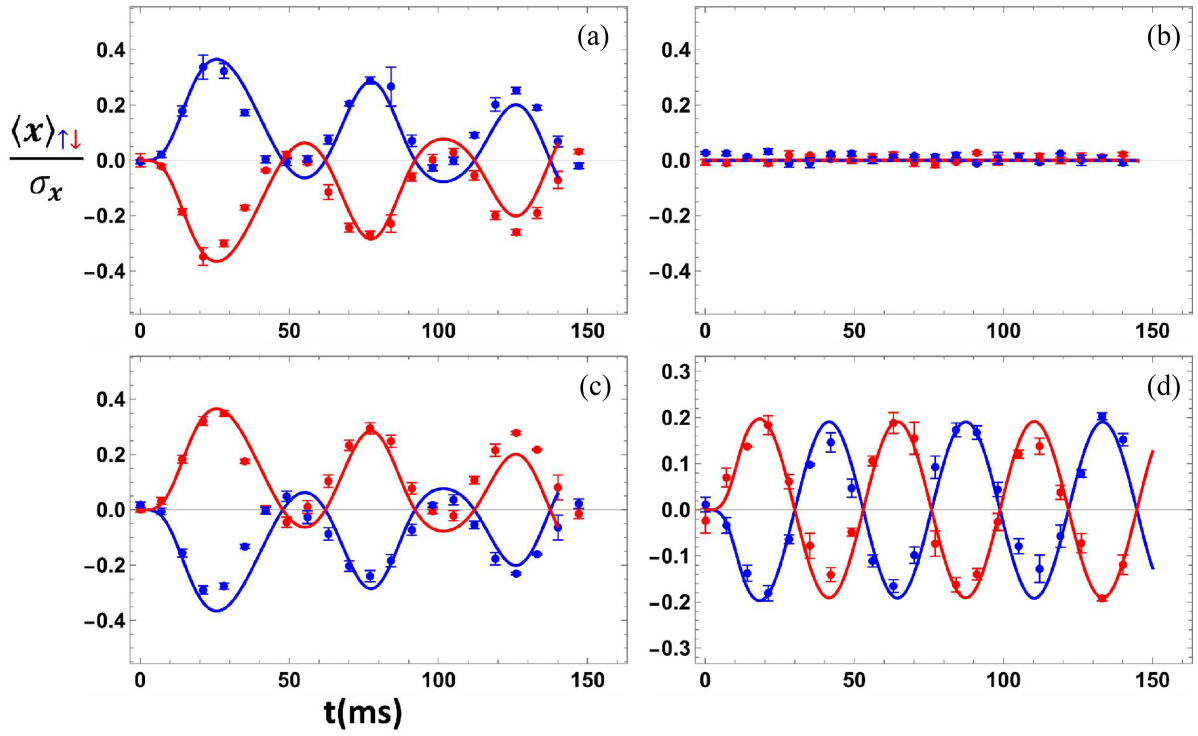

FIG. 3. Oscillating spin current versus chirality. $\langle x\rangle_{\uparrow\downarrow}$ denotes the center of mass of each spin state (blue and red) [24]. The s-wave scattering length is fixed at $a_s = -53.1a_0$. Chirality is controlled by the offset x_{os}; see Fig. 1. (a) $x_{os} = 0.8\sigma_x$; (b) $x_{os} = 0.0$; (c) $x_{os} = -0.8\sigma_x$; (d) $x_{os} = -3.0\sigma_x$, where $\sigma_x \simeq 200$ μm. Time is measured from the end of the $\pi/2$ RF pulse. The peak total density (a)–(c) is $\bar{n}_0 = 0.9/\mu\text{m}^3$, $\nu_x = 25.9$ Hz; (d) $\bar{n}_0 = 0.42/\mu\text{m}^3$, $\nu_x = 21.8$ Hz. The spin components reverse roles with the sign of x_{os}. Solid curves show predictions.

motion of the spins are interchanged when the sign of x_{os} is reversed [Figs. 3(a) and 3(c)]. With $x_{os} = \pm 0.8\sigma_x$, the spin-up and spin-down profiles separate, return to the center, and appear to bounce off of one another. In contrast, for $x_{os} = -3\sigma_x$, Fig. 3(d), the centers of mass oscillate completely through one another.

For $x_{os} = 0$, symmetrical spin segregation has been observed in the spin density profiles [12,22,25,26], where spin-up (-down) atoms appear to move to the center (edges) of the trap, reversing roles with the sign of the scattering length a_s. For the very small $a_s < 10a_0$ used in previous experiments [12,22,25,26], the evolution time of the spin density is long compared to the trap period. Then, the system can be modeled as an energy-space lattice [12,22] with effective long range interactions that arise from time-averaged s-wave scattering between atoms oscillating in the trap [27]. With $x_{os} = 0$, where $\langle\Omega\rangle \propto \langle x^2\rangle \propto E$ from Eq. (3), the spin vectors are correlated with the energy, yielding spatially symmetric spin density profiles [12,22,26,28–31].

In the present Letter, we observe tunable spin center of mass motion for $x_{os} \neq 0$ on timescales that are fast compared to the trap period, the opposite limit, by employing larger scattering lengths $a_s > 50a_0$ and spin rotation rates that can exceed the trap frequency. Here, the effective long range interaction picture is not valid, and the spin density profiles are spatially asymmetric.

We employ a 1D mean field treatment [14] of the weakly interacting cloud, where momentum-changing collisions can be neglected for the measurement timescale. The Heisenberg equations of motion are used to determine the evolution of the spin density components $(s_x, s_y, s_z) \equiv \mathbf{s}$ and the corresponding spin current densities $(J_x, J_y, J_z) \equiv \mathbf{J}$ in a one-dimensional approximation, where the direction of $\mathbf{J}$ denotes the direction of the spin carried by the current flowing along the x-axis. For our experimental parameters, forces arising from spatial derivatives of the mean field potential are negligible, as is the difference of the magnetic forces. In this case, the evolution equation for the total density shows that $n(x,t) = n_\uparrow(x,t) + n_\downarrow(x,t) = n_0(x)$ is time independent, as observed in the experiments. With these approximations, and assuming a local Maxwell-Boltzmann momentum distribution at temperature T, the spin density $\mathbf{s}(x,t)$ and current $\mathbf{J}(x,t)$ obey

$$\dot{\mathbf{s}} + \partial_x \mathbf{J} = \mathbf{\Omega} \times \mathbf{s}, \tag{4}$$

$$\dot{\mathbf{J}} + \frac{k_B T}{m}\partial_x \mathbf{s} + \omega_0^2 x\, \mathbf{s} = \mathbf{\Omega} \times \mathbf{J} - \frac{8\pi\hbar a_s}{m}\mathbf{s} \times \mathbf{J}. \tag{5}$$

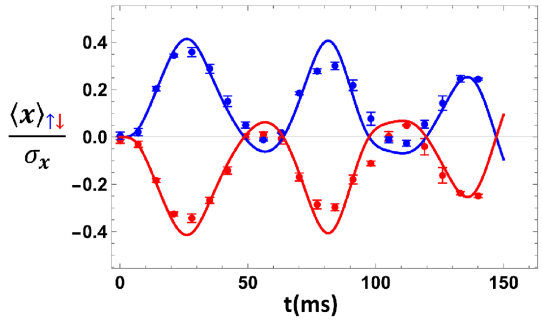

FIG. 4. Oscillating spin current [24] for an s-wave scattering length $a_s = -84.6a_0$ ($B = 500$ G). The chirality parameter (see Fig. 1) is $x_{os} = 1.15\sigma_x$ with $\sigma_x = 197$ μm, and $\bar{n}_0 = 0.99/\mu\text{m}^3$ with $\nu_x = 22.4$ Hz.

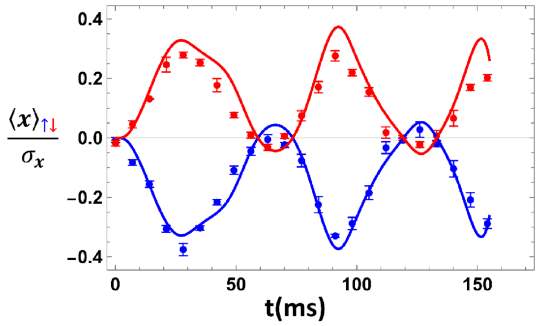

FIG. 5. Oscillating spin current [24] for an s-wave scattering length $a_s = -213.1a_0$ ($B = 437$ G). The chirality parameter (see Fig. 1) is $x_{os} = -0.8\sigma_x$ with $\sigma_x = 195$ μm, and $\bar{n}_0 = 0.52/\mu\text{m}^3$ with $\nu_x = 24.3$ Hz.

Here, $\mathbf{\Omega}$ [Eq. (3)] models the twist, and $a_s\mathbf{s}\times\mathbf{J}$ governs the spin-selective mean field rotation rate of $\mathbf{J}$ about $\mathbf{s}$.

Just after the $\pi/2$ radio-frequency pulse, the only nonvanishing initial condition is $s_x(x,0) = \frac{1}{2}n_0(x)$, where $n_0(x) = \bar{n}_0\exp(-x^2/\sigma_x^2)$ and $k_BT/m = \omega_0^2\sigma_x^2/2$. The s-wave scattering lengths at each magnetic field are calculated from the online data of Ref. [32]. The one-dimensional approximation implies that the strength of the $\mathbf{s}\times\mathbf{J}$ interaction term, which is proportional to the square of the density, should be averaged over the transverse dimensions. To fit the data, we find that the average peak 3D density $\bar{n}_0$ lies between $n_0/2$, as expected for a Gaussian distribution, and n_0, the peak 3D density, calculated from the measured total atom number and cloud profile [14]. Numerical solution determines the spin density profiles, $n_{\uparrow,\downarrow}(x,t) = \frac{1}{2}n_0(x) \pm s_z(x,t)$, which requires that $\langle x\rangle_\downarrow = -\langle x\rangle_\uparrow$, as predicted previously [27] and observed in our experiments.

The z-components of Eqs. (4) and (5) show that the centers of mass obey driven oscillator equations [14],

$$\partial_t^2\langle x\rangle_\uparrow + \omega_0^2\langle x\rangle_\uparrow = -\frac{8\pi\hbar a_s}{mN_\uparrow}\int dx(\mathbf{s}\times\mathbf{J})_z, \qquad (6)$$

where the effective driving force on the right side has an opposite sign for the $\downarrow$ spin component. In Eq. (6), $N_{\uparrow,\downarrow} = \bar{n}_0\sigma_x\sqrt{\pi}/2$ for a Gaussian spatial profile.

Figure 3(d) shows the fit of the model for the smallest scattering length $a_s = -53.1a_0$ (511 G), lowest density, and largest offset $x_{os} = -3\sigma_x$. In this case, the spatially varying rotation rate $\mathbf{\Omega}$ is nearly linear in x and dominates the mean field rotation rate $\propto a_s$ in Eq. (5). After the $\pi/2$ pulse, atoms scatter from a transient spin spiral; see Fig. S2 [14]. The x and y components of $\mathbf{s}$ and $\mathbf{J}$ form and vanish quickly compared to the trap period $1/\nu_x$, due to the rapidly increasing spread in rotation angles for atoms at different positions. As spin exchange scattering vanishes for the resulting z-polarized spin density and current, the effective force on the right-hand side of Eq. (6) takes the form of a pulse near $t = 0$; see Fig. S1 [14]. This produces an impulsive oscillator response with a period near $1/\nu_x = 45.8$ ms.

Figures 3(a), 3(c), 4, and 5 show the spin current obtained when the mean field rotation rate is larger than ν_x and comparable to or larger than the spread in $\mathbf{\Omega}$ across the trapped cloud. For these data, the model shows that the time-dependent effective force continuously modulates the oscillation amplitude and has a component that shifts the centers of oscillation, see Fig. S1 [14], causing the apparent bouncing. With increased s-wave scattering lengths, where $\mathbf{J}$ and $\mathbf{s}$ are more strongly coupled, the oscillation is distorted from pure sinusoidal.

In summary, our measurements demonstrate a general mechanism for manipulating the flow of spin current via asymmetric scattering in a chiral medium. The vanishing of s-wave scattering for parallel spins, according to the Pauli principle, makes the twisted Fermi gas cloud spin orienting. In chiral molecules, the CISS effect remains puzzling because the electron velocity through the crystal electric fields can be spin dependent even without atomic spin-orbit coupling. For the Fermi gas, there is no spin-orbit coupling, and the atom motion is unaffected, as the difference between the spin-dependent mechanical forces is negligible. Nevertheless, spatially asymmetric (chiral) spin waves appear as oscillations in the centers of mass of the spin components, driven by an effective force, which includes the back reaction of the spin current on the spin density. Our Letter motivates new Fermi gas quantum simulators with tailored chirality, which could include synthetic spin-orbit coupling [33].

Acknowledgments—We are pleased to acknowledge Professor Dali Sun for encouragement in this work. Primary support for this research is provided by the Air Force Office of Scientific Research (No. FA9550-22-1-0329). Additional support is provided by the National Science Foundation (No. PHY-2307107).

Data availability—The data that support the findings of this article are not publicly available. The data are available from the authors upon reasonable request.

[1] K. Ray, S. P. Ananthavel, D. H. Waldeck, and R. Naaman, Asymmetric scattering of polarized electrons by organized organic films of chiral molecules, Science **283**, 814 (1999).

[2] Z. Shang, T. Liu, Q. Yang, S. Cui, K. Xu, Y. Zhang, J. Deng, T. Zhai, and X. Wang, Chiral-molecule-based spintronic devices, Small **18**, 2203015 (2022).

[3] A.-M. Guo and Q.-F. Sun, Spin-selective transport of electrons in DNA double helix, Phys. Rev. Lett. **108**, 218102 (2012).

[4] B. Göhler, V. Hamelbeck, T. Z. Markus, M. Kettner, G. F. Hanne, Z. Vager, R. Naaman, and H. Zacharias, Spin selectivity in electron transmission through self-assembled monolayers of double-stranded DNA, Science **331**, 894 (2011).

[5] B. P. Bloom, Y. Paltiel, R. Naaman, and D. H. Waldeck, Chiral induced spin selectivity, Chem. Rev. **124**, 1950 (2024).

[6] H. Bentmann, Electron handedness in a material, Physics **18**, 113 (2025).

[7] T. Miki, H. Ikeda, M.-T. Suzuki, and S. Hoshino, Quantification of electronic asymmetry: Chirality and axiality in solids, Phys. Rev. Lett. **134**, 226401 (2025).

[8] A. Moharana, Y. Kapon, F. Kammerbauer, D. Anthofer, S. Yochelis, H. Shema, E. Gross, M. Kläui, Y. Paltiel, and A. Wittmann, Chiral-induced unidirectional spin-to-charge conversion, Sci. Adv. **11**, eado4285 (2025).

[9] R. Duine, Spinning fermions, Physics **1**, 27 (2008).

[10] A 0.5 ms $\pi/2$ pulse ensures uniform excitation, as the Rabi frequency $\Omega_R \simeq 3 \times 10^3\ s^{-1}$ is large compared to the spatially varying detuning of Eq. (3), where $\Omega_0 = 52.6\ s^{-1}$.

[11] Here, $\omega_\uparrow^2 - \omega_\downarrow^2 = -\omega_{\rm mag}^2 \partial_B E_{\uparrow\downarrow}(B)/\mu_B \simeq 2\omega_0 \delta\omega_{\uparrow\downarrow}$, with μ_B the Bohr magneton and $-E_{\uparrow\downarrow}(B) = E_2(B) - E_1(B)$ the energy difference for the two lowest ^{6}Li hyperfine states. $\omega_{\rm mag}$ is the measured oscillation frequency for either spin state in the magnetic potential. See Ref. [12].

[12] S. Pegahan, J. Kangara, I. Arakelyan, and J. E. Thomas, Spin-energy correlation in degenerate weakly interacting Fermi gases, Phys. Rev. A **99**, 063620 (2019).

[13] Strictly speaking, a spin spiral is produced by a z-dependent spin rotation about the z-axis, where $x \to z$ in the 1D model, giving identical behavior.

[14] See Supplemental Material at http://link.aps.org/supplemental/10.1103/73th-7hwt, which contains Refs. [15–18], for a discussion of the 1D mean field model, the effective force, and a table of the parameters used to model the data.

[15] J. E. Williams, T. Nikuni, and C. W. Clark, Longitudinal spin waves in a dilute Bose gas, Phys. Rev. Lett. **88**, 230405 (2002).

[16] M. O. Oktel and L. S. Levitov, Internal waves and synchronized precession in a cold vapor, Phys. Rev. Lett. **88**, 230403 (2002).

[17] C. Deutsch, F. Ramirez-Martinez, C. Lacroûte, F. Reinhard, T. Schneider, J. N. Fuchs, F. Piéchon, F. Laloë, J. Reichel, and P. Rosenbusch, Spin self-rephasing and very long coherence times in a trapped atomic ensemble, Phys. Rev. Lett. **105**, 020401 (2010).

[18] S. S. Natu and E. J. Mueller, Anomalous spin segregation in a weakly interacting two-component Fermi gas, Phys. Rev. A **79**, 051601 (2009).

[19] C. Lhuillier and F. Laloë, Transport properties in a spin polarized gas (I), J. Phys. (Paris) **43**, 197 (1982).

[20] J. N. Fuchs, D. M. Gangardt, and F. Laloë, Internal state conversion in ultracold gases, Phys. Rev. Lett. **88**, 230404 (2002).

[21] F. Piéchon, J. N. Fuchs, and F. Laloë, Cumulative identical spin rotation effects in collisionless trapped atomic gases, Phys. Rev. Lett. **102**, 215301 (2009).

[22] X. Du, Y. Zhang, J. Petricka, and J. E. Thomas, Controlling spin current in a trapped Fermi gas, Phys. Rev. Lett. **103**, 010401 (2009).

[23] In the initial experiments, we observed qualitatively that reversing the sign of the scattering length by tuning B above the zero crossing field $\simeq$527.18 G [12] interchanges the roles of the spin-up and spin-down profiles for the same x_{os}.

[24] Each data point is an average of four shots, taken in random time order. Error bars denote the standard deviation of the mean.

[25] X. Du, L. Luo, B. Clancy, and J. E. Thomas, Observation of anomalous spin segregation in a trapped Fermi gas, Phys. Rev. Lett. **101**, 150401 (2008).

[26] S. Smale, P. He, B. A. Olsen, K. G. Jackson, H. Sharum, S. Trotzky, J. Marino, A. M. Rey, and J. H. Thywissen, Observation of a transition between dynamical phases in a quantum degenerate Fermi gas, Sci. Adv. **5**, eaax1568 (2019).

[27] U. Ebling, A. Eckardt, and M. Lewenstein, Spin segregation via dynamically induced long-range interactions in a system of ultracold fermions, Phys. Rev. A **84**, 063607 (2011).

[28] A. P. Koller, M. L. Wall, J. Mundinger, and A. M. Rey, Dynamics of interacting fermions in spin-dependent potentials, Phys. Rev. Lett. **117**, 195302 (2016).

[29] M. L. Wall, Simulating fermions in spin-dependent potentials with spin models on an energy lattice, Phys. Rev. A **102**, 023329 (2020).

[30] J. Huang and J. E. Thomas, Energy-resolved spin correlation measurements: Decoding transverse spin dynamics in weakly interacting Fermi gases, Phys. Rev. A **109**, L041301 (2024).

[31] C. A. Royse, J. Huang, and J. E. Thomas, Collective dynamical Fermi suppression of optically induced inelastic scattering, Phys. Rev. Lett. **133**, 083404 (2024).

[32] G. Zürn, T. Lompe, A. N. Wenz, S. Jochim, P. S. Julienne, and J. M. Hutson, Precise characterization of ^{6}Li Feshbach resonances using trap-sideband-resolved rf spectroscopy of weakly bound molecules, Phys. Rev. Lett. **110**, 135301 (2013).

[33] V. Galitski and I. B. Spielman, Spin–orbit coupling in quantum gases, Nature (London) **494**, 49 (2013).